

On the stability of river bifurcations created by longitudinal training walls
Numerical investigation

Le, Binh; Crosato, Alessandra; Mosselman, Erik; Uijttewaal, Wim

DOI

[10.1016/j.advwatres.2018.01.012](https://doi.org/10.1016/j.advwatres.2018.01.012)

Publication date

2018

Document Version

Final published version

Published in

Advances in Water Resources

Citation (APA)

Le, B., Crosato, A., Mosselman, E., & Uijttewaal, W. (2018). On the stability of river bifurcations created by longitudinal training walls: Numerical investigation. *Advances in Water Resources*, 113, 112-125.
<https://doi.org/10.1016/j.advwatres.2018.01.012>

Important note

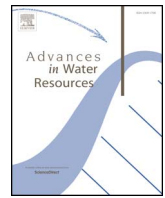
To cite this publication, please use the final published version (if applicable).
Please check the document version above.

Copyright

Other than for strictly personal use, it is not permitted to download, forward or distribute the text or part of it, without the consent of the author(s) and/or copyright holder(s), unless the work is under an open content license such as Creative Commons.

Takedown policy

Please contact us and provide details if you believe this document breaches copyrights.
We will remove access to the work immediately and investigate your claim.



On the stability of river bifurcations created by longitudinal training walls. Numerical investigation

T.B. Le^{a,b,*}, A. Crosato^{a,c}, E. Mosselman^{a,d}, W.S.J. Uijttewaalt^a

^a Delft University of Technology, PO Box 5048, 2600 GA Delft, The Netherlands

^b Thuy Loi University, 175 Tay Son, Dong Da, Hanoi, Viet Nam

^c UNESCO-IHE, Department of Water Engineering, PO Box 3015, 2601 GA Delft, The Netherlands

^d Deltare, Boussinesqweg 1, 2629 HV Delft, The Netherlands

ARTICLE INFO

Keywords:

Longitudinal training wall
River morphology
River bars
Bifurcation
Channel stability
Delft3D

ABSTRACT

To maintain a navigable channel and improve high-flow conveyance, engineers have recently proposed constructing longitudinal training walls as an alternative to the traditional transverse groynes. However, previous work has shown that the system of parallel channels created by a longitudinal training wall might be unstable in rivers with alternate bars. Many questions remain unanswered, particularly whether a stable system can be obtained by carefully designing the bifurcation point. This work analyses the stability of the bifurcating system created by a thin longitudinal wall in sand-bed rivers with alternate bars or point bars. The methodology includes performing 102 numerical tests using the Delft3D code to reproduce an idealized low-land river, either straight or meandering. The results show that the system of parallel channels separated by a training wall may indeed become unstable. An important factor is found to be the location of the bifurcation point with respect to a neighboring bar or point bar. The same trends are observed for both constant and variable discharge, in straight and meandering channels. The results suggest that cyclic growth and decline of the bifurcating channels may arise as inherent system behavior, without the need of any additional external forcing. We explain this from changes in the relationship between sediment transport ratio and discharge ratio as the bifurcation evolves. This cyclic behavior can be regarded as a form of system stability and can be obtained by carefully placing the starting point of the longitudinal training wall, and thus the bifurcation point, near the top of a bar.

1. Background and objective

Lowland rivers have been trained for centuries with transverse groynes to prevent bank erosion and to improve and maintain a navigable channel. Longitudinal training walls are less commonly applied, but they can serve the same purposes.

In the Netherlands, series of transverse groynes have been built to prevent ice jams during the winter and improve channel navigability by channel narrowing (Fig. 1a). The large-scale narrowing of the Rhine branches, along with bend cutoffs and sediment mining, triggered a morphological response of incision at rates up to over 2 cm/year. Apart from draining riparian habitats in floodplains and undermining hydraulic structures, this incision also deteriorated the conditions for navigation. To mitigate these effects, groynes in the river Waal near Tiel were replaced by longitudinal training walls in the years 2013–2015, as a pilot for testing this alternative approach to river training (Fig. 1b). The main idea was to provide a narrow and, hence, deep main channel during low flows, while allowing more water to flow in the secondary

channel behind the training wall at higher discharges in order to reduce main channel erosion and to lower the water levels during floods. Furthermore, the presence of the secondary channel was expected to improve the ecological conditions of the river. Finally, the fairway would no longer be spoiled by the shallow ridges that develop in response to the formation of local scour holes at groyne heads.

Another pertinent example is the Quang Ngai irrigation system in central Vietnam which was built in the period 1985–1997 in the framework of the Thach Nham project. It comprises two main intakes upstream and many small free inlets further downstream along both sides of the Tra Khuc River. During the dry season the main low-flow stream sways inside the main channel changing location every year (Fig. 2). This creates the need to guarantee water flow to the intakes without hindering the water conveyance during the rainy season. Two solutions are proposed to solve the problem. The first one is to move the intakes to other locations where the main stream is more stable. The second solution proposes constructing longitudinal training walls along the river banks in the reach with the intakes. This solution is expected

* Corresponding author at: Delft University of Technology, Mekelweg 2, 2628 CD Delft, South Holland, The Netherlands.
E-mail address: t.b.le@tudelft.nl (T.B. Le).

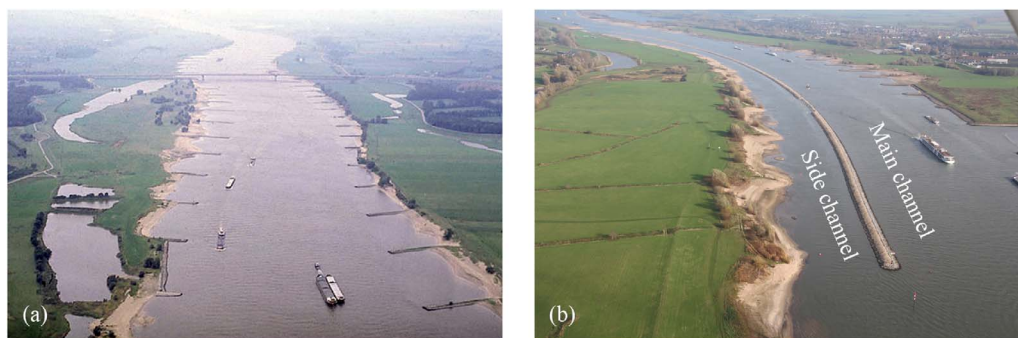


Fig. 1. (a) Classical transverse groynes versus (b) longitudinal training wall in the Waal River near Tiel. Source: Rijkswaterstaat.



Fig. 2. Tra Khuc River (Vietnam). The small branch on the right might become the main low-flow stream in the future (photograph Le Thai Binh).

to be more easily accepted by the local community, since it would not change the old channel system and the land use along the river. Therefore, longitudinal training walls appear as a promising solution to clear the entrances of water inlets and intakes along the Tra Khuc River.

A longitudinal training wall divides a river in two parallel channels, usually having different widths, with an upstream bifurcation. As river bifurcations are often unstable, the question arises whether the two-channel system will be stable and, in case of instability, which channel would silt up. The pattern of steady bars in the river can be assumed to be a major factor for this stability, because bars influence the sediment distribution between the two channels (De Heer and Mosselman, 2004; Redolfi et al., 2016; Le et al., 2018). We address this question in the present research by carrying out a long series of numerical tests using the Delft3D code, considering that this code has already proven to be successful in simulating the morphological development of this type of systems (Le et al., 2018). The objective is to assess the stability of the channels on either side of a longitudinal training wall in single-thread sand-bed rivers with steady or slowly migrating alternate bars or point bars. Several cases are considered: different locations of the bifurcation point with respect to a bar or point bar, different channel widths, constant and variable discharges, as well as straight and sinuous channels.

2. Theoretical background

2.1. Stability of bifurcations and bars

Bifurcation stability depends on the flow and sediment transport in the upper reaches of the branches below the bifurcation. If more sediment enters the branch than the flow can transport, the branch will experience sedimentation. If less sediment enters, the bed of the branch will erode. If the amount of sediment entering each branch is exactly equal to the transport capacity of the flow, the bifurcation is in equilibrium. This equilibrium is stable if it is restored after a small perturbation, e.g. if occasional erosion in a branch generates sediment overloading, producing counteracting sedimentation. It is unstable if the small perturbation grows further, for instance if occasional erosion in a branch generates a shortage of sediment entering this branch, giving rise to further erosion.

The stability of a bifurcation is therefore governed by the interplay between the distributions of water and sediment between the two branches. These distributions depend on the structure of flow and sediment transport in the area immediately upstream of the bifurcation. Most alluvial rivers have wavy channel beds due to the presence of bars (Fig. 3). This makes the structure of flow and sediment transport



Fig. 3. Examples of bars in low-land rivers. (a) Han River in Danang, Vietnam. © Google Earth, 2015. (b) Cauca River, Colombia (photograph Erik Mosselman).

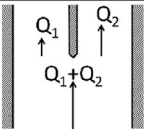
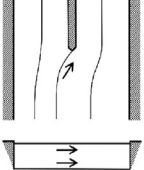
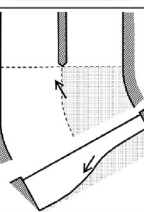
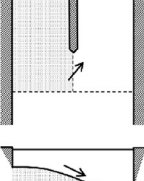
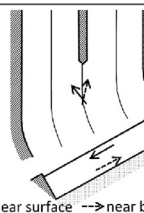
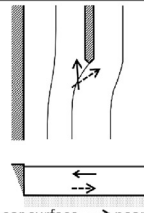
Mechanism		Inclusion in nodal point relation *				
		WFVL	BRT	KJMS	BZMRT	MM
	Discharge distribution	+	+	+	+	+
	Transverse velocity due to redistribution of flow over cross-section	-	+	+	+	+
	Transverse bed slope due to upstream bars (e.g. point-bars in bends or alternate bars in straight reaches)	-	-	-	+	-
	Transverse bed slope due to downstream bed elevation difference	-	+	+	+	-
	Helical flow due to upstream bend	-	-	+	-	-
	Helical flow due to redistribution of flow over cross-section	-	-	-	-	+
* WFVL = Wang et al (1995), BRT = Bolla Pittaluga et al (2003), KJMS = Kleinhans et al (2008), BZMRT = Bertoldi et al (2009), MM = Van der Mark & Mosselman (2013)						

Fig. 4. Mechanisms affecting the distribution of sediment at bifurcations and their incorporation in sediment distribution relationships for 1D models.

complex. Bars are associated with lateral flow redistribution, transverse bed slopes and helical flow that alter the sediment transport direction (Struiksmas et al., 1985). These features affect the distribution of sediment at bifurcations (Bertoldi and Tubino, 2007). The presence of a bar, and in particular a steady bar (Redolfi et al., 2016; Le et al., 2018), might therefore lead to the silting up and closure of one of the two parallel channels divided by the longitudinal wall.

Bars develop due to either morphodynamic instability occurring at sufficiently large width-to-depth ratios or morphodynamic forcing, or both. The bars that arise from morphodynamic instability are called “free bars”. These bars are typically periodic and can migrate in downstream or in upstream direction (Zolezzi and Seminara, 2001; Zolezzi et al., 2005; Mosselman et al., 2006). The linear stability analyses carried out since the 1970s show that a flat alluvial bed may develop into a pattern of alternate or multiple bars (unstable bed), depending on the flow width-to-depth ratio and other morphodynamic

parameters (e.g., Hansen, 1967; Callander, 1969; Engelund, 1970; Engelund and Skovgaard, 1973; Parker, 1976; Fredsøe, 1978). Zolezzi and Seminara (2001) showed that free bars migrate in downstream direction if the flow width-to-depth ratio is smaller than the resonant one (sub-resonant conditions), and in upstream direction if it is larger (super-resonant conditions). At resonant conditions free bars present zero celerity. Notwithstanding the presence of simplifying assumptions, such as a constant discharge, the results of these analyses are successfully used as physics-based predictors of the alluvial channel pattern (e.g. Parker, 1976; Lanzoni, 2000; Crosato and Mosselman, 2009).

“Morphodynamic forcing” is the result of permanent flow curvature that arises from a local change of channel geometry, which can be caused by a bend, a structure, and a local width change. Curved flow results in outer-bend scour and inner-bend sediment deposition. Typical “forced bars” are the point bars that become visible during low flows at

the inner side of river bends.

Forcing can also fix the location of free bars (Struiksma et al., 1985; Struiksma and Crosato, 1989). Such bars with zero celerity can give rise to a more extensive pattern of periodic non-migrating sediment deposits. These deposits are called “hybrid bars” because they depend on both forcing and morphodynamic instability (Duró et al., 2015). Recent theoretical analyses show that steady bars may arise upstream of the bifurcation point as a result of the perturbation generated by the start of the longitudinal wall if the original channel exceeds the width-to-depth ratio that allows for upstream morphodynamic influence, i.e. is at super-resonant conditions (Redolfi et al., 2016).

Forced and hybrid bars are rather common in low-land rivers, since natural channels are generally irregular, resulting in numerous forcings, and this is why the presence of these bars is considered central in this study.

2.2. Bifurcation stability analyses

Non-linear phase-plane stability analyses of one-dimensional bifurcation models by Flokstra (1985) and Wang et al. (1995) show how sensitive bifurcations are to the distribution of sediment transport. These analyses use simple hypothetical relationships in which the ratio of sediment transports into the two branches is a function of the ratios of discharges and widths of the two branches:

$$\frac{Q_{s1}}{Q_{s2}} = \left(\frac{Q_1}{Q_2}\right)^k \left(\frac{B_1}{B_2}\right)^{1-k} \quad (1)$$

where Q_{s1} and Q_{s2} are the sediment transport rates entering branch 1 and 2, respectively; Q_1 and Q_2 are the water discharges; B_1 and B_2 are the channel widths; and k is a number that has to be determined empirically. For low values of k , this relation is destabilizing, because a higher discharge into one branch would generate a higher (stabilizing) sediment input but an even higher (destabilizing) sediment throughput due to the nonlinear relation between sediment transport capacity and discharge. The stabilizing effect of the higher sediment input prevails only if k is sufficiently large. Wang et al. (1995) found that bifurcations are stable (both channels remain open) for $k > 5/3$ and unstable (one of the channels silts up) for $k < 5/3$ if the sediment transport capacity is computed with Engelund and Hansen's (1967) formula, which is valid for sand-bed rivers.

In principle, 2D and 3D models can be used to calculate the distribution of sediment transport into the branches of a bifurcation. In 1D models, however, the 2D and 3D details of flow and sediment transport at the bifurcation are lost. Several researchers attempted to improve the relationships for sediment transport distribution over bifurcated branches in 1D models by accounting in a parameterized way for various mechanisms that may play a role (Fig. 4).

Bolla Pittaluga et al. (2003) extended Wang et al. (1995) formula by incorporating transverse flows due to the redistribution of discharges over the cross-section and by incorporating the effects of transverse bed slope in the final reach of the upstream channel with normal width, flow discharge and sediment transport rate equal to B_0 , Q_0 and Q_{s0} , respectively. The additions by Bolla Pittaluga et al. (2003) imply that more sediment is transported towards the largest and deepest channel downstream. They thus have a stabilizing effect. Indeed, Bolla Pittaluga et al. (2003) found that for low values of the flow width-to-depth ratio and large values of the Shields parameter of the flow, symmetrical bifurcation geometries are stable. As the width-to-depth ratio increases (or the Shields number decreases) this configuration loses stability. De Heer and Mosselman (2004) commented that the relationship of Bolla Pittaluga et al. (2003) does not account for upstream asymmetries, such as the presence of bars. They expressed the expectation that an extension with more mechanisms of sediment distribution would reveal that bifurcations can be unstable under more conditions than suggested by the analysis of Bolla Pittaluga et al. (2003). Such

extensions were proposed subsequently by Kleinhans et al. (2008), Bertoldi et al. (2009) and Van der Mark and Mosselman (2013).

Bertoldi et al. (2009) included the effect of migrating bars according to relations by Colombini et al. (1987) for free alternate bars that occur in long straight channels with uniform width. Bars arriving at the bifurcation feed the downstream branches alternately with a larger amount of water and sediment. The time period of this feeding is set by the ratio between bar length and migration speed. As a result, the bifurcation oscillates around an equilibrium or disappears due to closure of one of the branches. The findings of Bertoldi et al. (2009) do not hold, however, for the point-bars and hybrid steady bars that are encountered more generally in rivers than free bars.

Kleinhans et al. (2008) added the effects of helical flow in upstream river bends to the sediment distribution relation of Bolla Pittaluga et al. (2003) by modifying the direction of the sediment transport affected by transverse slope. However, the transverse bed slope is still calculated from the elevation difference between the bed levels in the downstream branches, not from the topography of the upstream point-bar that is formed in alluvial river bends.

Van der Mark and Mosselman (2013) proposed a relationship for the effects of helical flow in which the streamline curvature generating this helical flow is related to redistribution of the flow over the cross-section rather than related to an upstream river bend. They tested their relationship as well as other relationships against field data, concluding that all relationships perform poorly and that reliable models of river bifurcations should be at least two-dimensional. Systematic 2D numerical simulations by Kleinhans et al. (2008) shed more light on the effects of different sediment distribution mechanisms on bifurcation stability. Unstable bifurcations can be nearly balanced if mechanisms favoring the closure of one channel are compensated by mechanisms favoring the closure of the other channel. Such nearly balanced bifurcations develop more slowly than unbalanced bifurcations. Furthermore, the numerical simulations showed the sediment distribution relationships to change as a bifurcation evolves. In this way an initially unstable bifurcation may become stable in a strongly asymmetrical configuration, without reaching full closure of the declining branch.

3. Numerical investigations

3.1. Model description

We analysed the results of a large number of 2D numerical simulations reproducing the behavior of an idealized low-land river with alternate bars or point bars which is divided into two parallel channels by a thin longitudinal wall.

The Delft3D code solves the three-dimensional Reynolds equations for incompressible fluid and shallow water with a finite-difference scheme (Deltares, 2014). A variety of sediment transport formulas is available to compute the sediment transport rate. Bed level changes are derived by either applying the Exner principle (bed load or fast adapting suspended load) or from a sediment balance equation in which sediment deposition and entrainment rates are derived as a function of suspended-solid concentrations and hydrodynamic parameters. The models developed in the framework of this study were based on the depth-averaged version of the basic equations (2D approach). Defina (2003), Schuurman et al. (2013), Duró et al. (2015) and Singh et al. (2017) demonstrated that this type of approach is able to simulate bar processes with sufficient accuracy. The approach is also supported by the experience of Le et al. (2018), who successfully reproduced the long-term morphological developments of this type of systems at the laboratory scale with a 2D model built using the Delft3D code.

3.2. Model setup

We selected values of the hydraulic and morphological variables

Table 1
Characteristics of the Waal River and numerical simulations in this study.

Parameters	Notation	Unit	Waal River	Computational case
<i>Hydrological characteristics</i>				
Average discharge	$Q_{50\%}$	m^3/s	1587	200
Minimum discharge	Q_{min}	m^3/s	939	118
Maximum discharge	Q_{max}	m^3/s	4680	590
Discharge ratio between Q_{max} and Q_{min}	Q_{max}/Q_{min}	–	4.98	5.00
Discharge ratio between Q_{max} and $Q_{50\%}$	$Q_{max}/Q_{50\%}$	–	2.95	2.95
<i>1D hydraulic and morphological characteristics at average discharge</i>				
River width	B_0	m	250	90
Normal depth	h	m	6.0	3.0
Longitudinal bed slope	i	–	10^{-4}	10^{-4}
Chézy coefficient	C	$\text{m}^{1/2}/\text{s}$	43	43
Froude number	Fr	–	0.137	0.137
Shields parameter	θ	–	0.365	0.906
Median sediment grain size	D	m	1.0×10^{-3}	2×10^{-4}
Relative density of sediment	Δ	–	1.65	1.65
Transport law	Engelund-Hansen (1967)			
<i>2D hydraulic and morphological characteristics at average discharge</i>				
Width-to-depth ratio	B/h	–	42	30
Theoretical bar mode	m	–	1	1
(Crosato and Mosselman, 2009)				

and parameters that represent a “typical lowland river with alternate bars or point bars”. Such variables and parameters were inspired by the Waal River in the Netherlands (Fig. 1) and are listed in Table 1. The computational case, however, is not a scaled version of the Waal River, since the two systems differ, for instance in the value of the Shields parameter.

Fig. 5 shows part of the numerical grids (45 km total length) for the straight and the sinuous channel, the rectangular grid size being $15 \times 45 \text{ m}^2$ (straight channel). In all models $B_0 = B_1 + B_2$ where B_0 is the original river width, B_1 is the side (smaller) channel width and B_2 is the main (larger) channel width. Three width combinations are investigated, including the scenario in which $B_1 = B_2$. In the curved channel, the wavelength of the meanders along the straight line connecting their inflection points was chosen to be equal to the equilibrium hybrid-bar wavelength (1350 m). The meander amplitude was equal to 100 m.

The hydrodynamic boundary conditions of the models consisted of downstream water level and upstream discharge. These boundary conditions were either constant (most scenarios), with a discharge of $200 \text{ m}^3/\text{s}$, or variable. The discharge hydrograph adopted in the

variable-discharge scenarios was inspired by the Waal River (Table 1). The typical hydrological year is depicted in Fig. 6. The boundary conditions for the sediment component were upstream balanced sediment transport, which prevented the bed level from changing at the boundary, and a downstream free sediment transport condition, which allows undisturbed level changes up to the boundary. The banks were kept fixed and treated as free-slip boundaries.

The morphodynamic conditions of the simulated system correspond to a river channel with alternate bars. The theoretical mode m is the integer representing the type of bars that form in the river channel; it was here computed according to Crosato and Mosselman's (2009) theory. The value $m = 1$ (Table 1) refers to alternate bars. Applying the linear theory, both the Waal River at average discharge and the computational case result in super-resonant conditions, but very close to resonance (Blondeaux and Seminara, 1985). In such a case, a finite flow discontinuity near the upstream boundary leads to the formation of a series of hybrid alternate bars (Struiksma and Crosato, 1989; Mosselman et al., 2006). Such a discontinuity was obtained in the straight channel simulations by placing a transverse thin dam obstructing $1/2$ of the channel width at a distance of 900 m from the upstream boundary, ten times the width of the channel B_0 . The sinuous-channel simulations did not need an external disturbance to obtain the formation of point bars which spontaneously form at the inner side of bends.

The longitudinal training wall was schematized as a thin, infinitely high and deep, dam to ensure that the structure always divides the two channels, even at the highest flow rates.

The bed roughness was represented by a constant Chézy coefficient (value in Table 1) and the bed-load transport rate was computed by means of the Engelund-Hansen (1967) formula, valid for sand bed rivers. The bed slope effect on sediment transport direction was taken into account in all simulations (Mosselman and Le, 2016). Two formulations were considered: Bagnold's (1966) (default in Delft3D) and Koch and Flokstra's (1981). Koch and Flokstra's formulation was adopted solely for the sensitivity analysis meant to study the effects of transverse bed slope on bifurcation stability, since it allows having a stronger vs. smaller effect of transverse bed slope on sediment transport direction by changing the value of one or more coefficients. The influence of the spiral flow in curved reaches was accounted for according to the formulation of Struiksma et al. (1985).

In Delft3D, the drying of wet cells is imposed based on a threshold water depth. Cells that become dry are removed from the hydro-morphological computational domain and remain dry. They may become wet again by bank erosion, but this is not considered in our computations. In our simulation this threshold water depth was 10 cm (default in Delft3D).

The time step of the flow computations was 0.5 min to ensure numerical stability and accuracy, as evaluated by the criterion that the

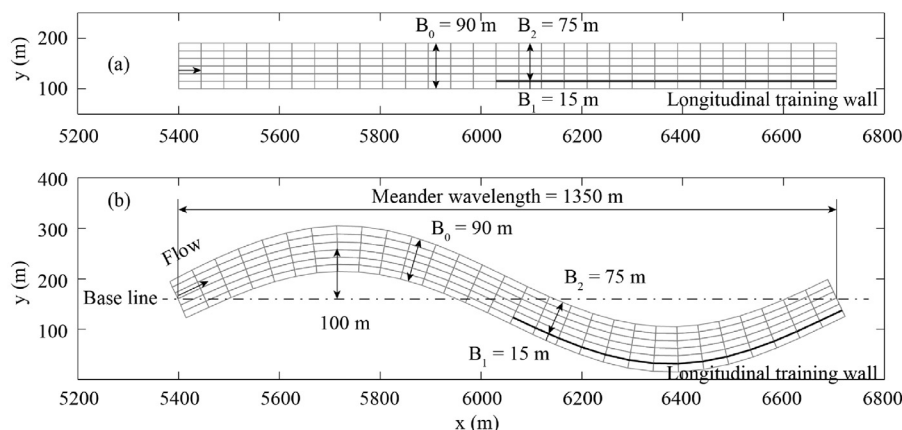


Fig. 5. Numerical grid and longitudinal training wall for $B_1:B_2 = 1:5$. (a) Straight channel models. (b) Sinuous channel models.

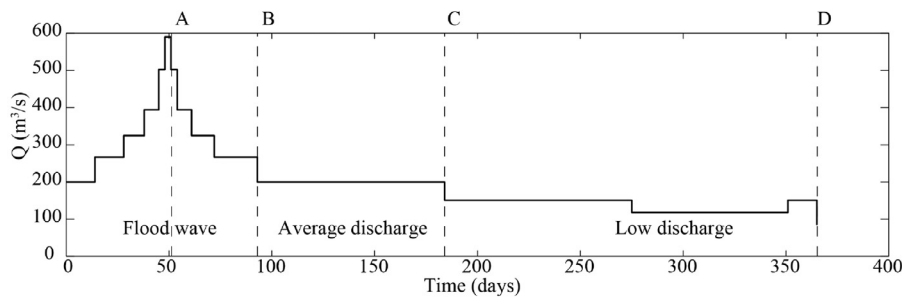


Fig. 6. Discharge hydrograph used in the variable-discharge scenarios (average discharge = $200 \text{ m}^3/\text{s}$). A, B, C, D indicate the moments of the plots in Fig. 13.

Courant number is smaller than 10.

The morphological developments in all simulations with constant discharge were accelerated by using a morphological acceleration factor (MF) equal to 10, after having checked that this does not affect the results in a way that is relevant for the scope of the study. This approach is also justified because previous studies in river channels with similarly small Froude numbers (e.g. Crosato et al., 2011; Duró et al., 2015) showed that it hardly affects the development of the 2D bed topography in a river with hybrid bars. For the simulations with variable discharge, we did not accelerate the computations (MF = 1). As a result, the running times were 10 years for all constant discharge scenarios (with MF = 10) and 100 years for the variable discharge scenarios (with MF = 1). This means that we computationally cover 100 years in all cases. The computational time proved to be long enough to reach a new morphodynamic equilibrium, characterized by negligible temporal changes of the average bed elevation of the parallel channels (see Chapter 4). Table 2 summarizes the numerical parameters used in the simulations.

3.3. Model runs

The investigation comprises 102 different model runs. These are meant to study the effects on bifurcation stability of: longitudinal wall starting point (Runs W_0); width ratio (Runs W_0 , W_1 and W_2); and variable discharge (Runs V_0 , V_1 and V_2 , with different width ratios). The investigation includes a sensitivity analysis to assess the effects on bifurcation stability of the deviation of bed load direction due to transverse bed slope (Runs A). In addition, four runs are carried out to study bifurcation stability in a sinuous channel (Runs S). These are especially meant to investigate whether accounting for the effects of spiral flow on bed load direction may result in different morphological trends, since spiral flow deviates bed load transport in opposite direction compared to transverse bed slope (Struiksmma et al., 1985; Kleinhans et al., 2008; Ottevanger, 2013). The performed simulations are listed in Table 3.

All scenarios included a reference case without longitudinal wall, but with a transverse wall to generate the initial bed topography with alternate hybrid bars. This bed topography is then the starting condition of all the other runs. To study the influence of bars on the stability of the bifurcation created by the start of the longitudinal wall, several starting locations were identified with respect to a selected steady bar

(Fig. 7). These locations are numbered from 1 to 18 (Location 18 corresponds to Location 1 with respect to the next bar). The effects of the starting location were then analysed for different width ratios, namely: $B_1: B_2 = 1:5$ (W_0) - base-case scenario; 1:2 (W_1) and 1:1 (W_2) (see Table 3).

4. Results

4.1. Effects of starting location

The 18 simulations reproducing the long-term morphological developments of the base-case scenario (W_0 runs with $B_1: B_2 = 1:5$ and constant discharge) differ solely in the starting location of the longitudinal wall. The results show that if the training wall starts in the upstream part of a steady bar, i.e. at Locations 3–7, the side channel silts up (Fig. 8b). Instead, if the training wall starts in the downstream part of the bar, i.e. at Locations 11–17, the side channel deepens and it is the main channel that silts up. In this case, the side channel eventually conveys almost all the water discharge (Fig. 8d).

A different morphodynamic behavior is observed if the training wall starts near the bar top, at Locations 8–10. In this case, the results show a dynamic balance in which the side channel experiences cycles of erosion and sedimentation and remains open (Fig. 8c). Every cycle comprises three steps (Fig. 9): 1) rise of side-channel bed; 2) bar formation near the upstream end of the side channel and side-channel bed erosion; 3) upstream bar erosion and return to the initial state. These cycles repeat continuously during the 100 years covered by the computations. The first cycle is illustrated in Fig. 9.

The simulated systems were slightly super-resonant at average flow. In this case, the perturbation caused by the starting of the longitudinal wall might affect the shape of the steady bars upstream (Redolfi et al., 2016). However, the obtained results do not always show upstream influence of the bifurcation point. Indeed, when the training wall starts in the upstream part (Fig. 8b) or near the bar top (Fig. 8c), upstream bars do not show any changes compared to the reference case (Fig. 8a). When the training wall starts in the downstream part, a bar deformation extends to a distance upstream of about 3 bar wavelengths (Fig. 8d). Independently from the bifurcation point, no bars formed upstream of the transverse forcing dam that was placed to generate the series of hybrid bars downstream (not in the figures).

Fig. 10a shows the temporal variations of the proportion of total discharge that flows in the side channel, Q_1/Q_0 , in some representative cases. If $Q_1/Q_0 = 0$ all the discharge is conveyed by the main channel. If $Q_1/Q_0 = 1$ all the discharge is conveyed by the side channel. The fastest developments pertain to the cases in which the side channel becomes increasingly deep.

Fig. 10b shows the variations of sediment transport ratio versus discharge ratio during the computations, the initial discharge ratio Q_1/Q_2 being about 1/8. This figure shows also theoretical sediment transport ratios as a function of Q_1/Q_2 for $B_1: B_2 = 1:5$ (base-case scenario), computed using Eq. 1 (Wang et al., 1995). In the logarithmic-scale graph, the values of the exponent k are represented by the slope of the straight lines. According to Wang et al., the bifurcation is stable

Table 2
Values of numerical parameters used in the simulations.

Parameters	Notation	Unit	Value
Size of computational domain	$L \times B$	$\text{m} \times \text{m}$	$45,000 \times 90$
Rectangular size of grid cell	–	$\text{m} \times \text{m}$	45×15
Number of grid cells	$M \times N$	–	1000×6
Time step	t	s	30
Simulation time	T	year	100
Running time and morphological factor	T_{run} & MF	–	10, MF = 10 (constant discharge) 100, MF = 1 (variable discharge)

Table 3
Overview of the simulations in this study.

Run	Scenarios	Starting location	Width ratio* $B_1:B_2$	Initial bed level	Descriptions
<i>Constant discharge (55 simulations)</i>					
Reference case with constant discharge			No wall	Flat bed	Reference run to obtain hybrid steady bars with constant discharge and Bagnold's (1966) formulation
W ₀	Width ratio 0 (base-case constant discharge)	1–18	1:5	Hybrid bars	W runs study the effects of different width ratios and starting point of the longitudinal wall with respect to a hybrid bar
W ₁	Width ratio 1	1–18	1:2	Hybrid bars	
W ₂	Width ratio 2	1–18	1:1	Hybrid bars	
<i>Variable discharge (10 simulations)</i>					
Reference case with variable discharge			No wall	Flat bed	Reference run to obtain hybrid steady bars with variable discharge and Bagnold (1966) formulation
V ₀	Width ratio 0 (base-case variable discharge)	4, 10, 17	1:5	Hybrid bars	V runs study the effects of starting location considering that hybrid bars are expected to change due to discharge variation. Three width ratios are considered.
V ₁	Width ratio 1	4, 10, 17	1:2	Hybrid bars	
V ₂	Width ratio 2	4, 10, 17	1:1	Hybrid bars	
<i>Sensitivity analysis (33 simulations)</i>					
Reference case with constant discharge			No wall	Flat bed	Reference runs to obtain hybrid steady bars with constant discharge and Koch and Flokstra (1981) formulation.
A	Sensitivity analysis	4, 17	1:5	Hybrid bars	One run per value of A_{sh} ** A runs study slope effects of transverse slope on bed load direction. Two locations for each value of A_{sh}
<i>Sinuuous river (4 simulations)</i>					
Reference case with constant discharge			No wall	Flat bed	Reference run to obtain point bars inside bends
S	Sinuuous planform	4, 10, 17	1:5	Hybrid bars	S runs study the effects of spiral flow on a sinuuous river with constant discharge

* B_1 = side channel width and B_2 = main channel width.
** A_{sh} is a parameter in Koch and Flokstra (1981) formulation (see Section 4.4).

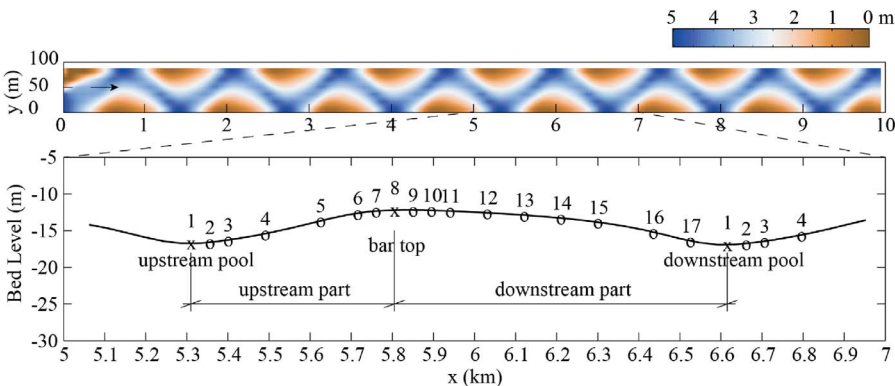


Fig. 7. Equilibrium state of bars and starting locations of the training wall with respect to a bar. Bar wavelength: 1350 m, bar amplitude: 2.85 m, $B/h = 30$. Upper graph: water depth at the constant discharge of 200 m³/s after 100 years. Lower graph: zoomed in longitudinal profile along the right bank from km 5 to km 7.

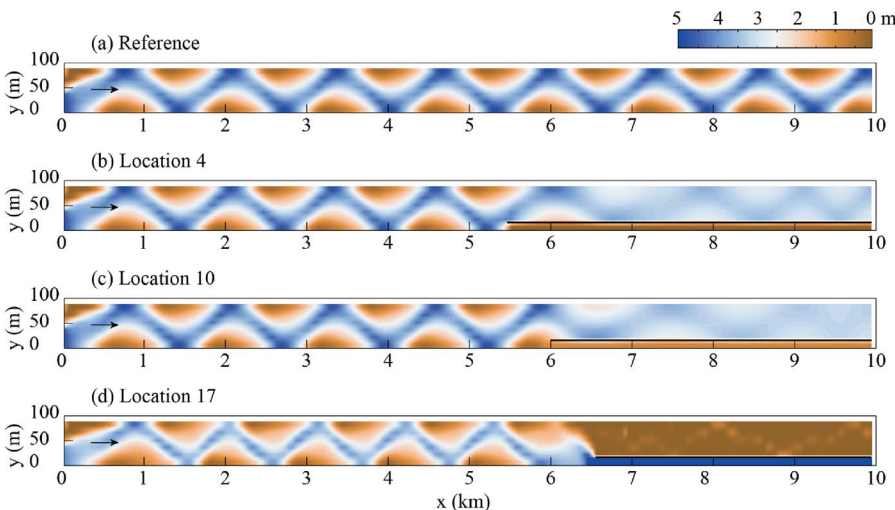


Fig. 8. Water depth at the constant discharge of 200 m³/s after 100 years (first 10 km after the transverse dam). (a) Reference case without training wall. (b) Training wall starting at Location 4: the side channel closes and bars in the main channel tend to disappear for a distance. (c) Training wall starting at Location 10: both channels remain open. (d) Training wall starting at Location 17: the side channel deepens and the main channel is closed.

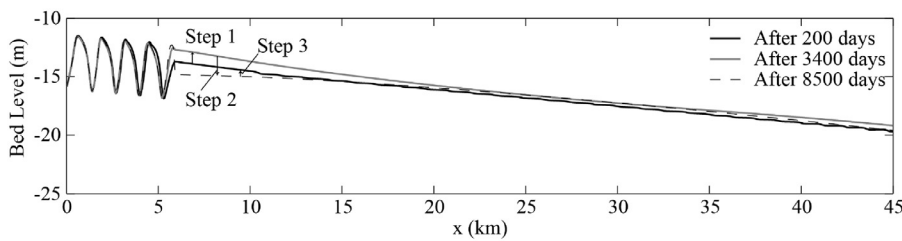


Fig. 9. Longitudinal bed level profile of the side channel when the training wall starts at Location 10: first cycle of dynamic balance.

(both channels remain open) for $k > 5/3$ and unstable (one of the channels silts up) for $k < 5/3$ in case sediment transport capacity is governed by the formula of Engelund and Hansen (1967). This is the transport formula adopted in the simulations. The application of Wang et al.'s theory implies deriving the constant value of k by calibration. For the performed numerical tests, this would lead to the selection of a value of k within the instability conditions for most cases. For location 10, however, the numerical results show that the system assumes a dynamic balance in which it alternates between a stable bifurcation, with a slope, k , in Fig. 10b that is steeper than $5/3$, and an unstable bifurcation, with a slope that is less than $5/3$. Temporal variations thus allow a limit cycle that is not a possible solution in the theoretical analysis of Wang et al. (1995) that uses a constant value of k . This suggests that an oscillating distribution of discharges can arise as inherent system behavior, not necessarily imposed by the alternating arrival of migrating bars from upstream as in Hirose et al. (2003) and Bertoldi and Tubino (2007) because in our system we do not have migrating bars at the longitudinal wall starting location. This behaviour can be theoretically described only when allowing for temporal variations of k in Wang et al. (1995) formula (Eq. (1)).

4.2. Effects of altering the width ratio between side and main channel

The results of the long-term morphological simulations show that altering the width ratio does not change the final result. The trends are the same as in the base-case scenario (Fig. 11): if the training wall starts in the upstream part of a hybrid bar the side channel silts up (Fig. 11a), instead, if the training wall starts in the downstream part of the same bar the side channel deepens and the main channel aggrades (Fig. 11c). If the training wall starts near the bar top, both channels remain open (Fig. 11b).

Fig. 12 shows the temporal variations of the proportion of total discharge that flows in the side channel (Q_1/Q_0) for various width ratios. If the training wall starts in the upstream part of a bar, the side channel silts up completely ($Q_1/Q_0 = 0$, dash-dot lines) as seen in the previous section. This happens for all considered width ratios, except for $B_1/B_2 = 1:1$ (side and main channel having equal width) where the process is slower (red line) and does not result in complete closure of one of the channels. If the training wall starts in the downstream part of a bar, the side channel eventually conveys most water discharge (dash

lines). It conveys 100% of the water (main-channel closure) only for $B_1/B_2 = 1:5$ (black line), whereas the main channel remains open for the larger width ratios ($B_1/B_2 = 1:2$ and $B_1/B_2 = 1:1$). However, also in these cases the side channel still conveys the major part of the discharge, with $Q_1/Q_0 > 0.95$. In the new equilibrium, bars are not observable in the deeper channel, whereas some low-amplitude bars are present in the silting-up channel. They are the remains of bars that formed during the transition period.

When the training wall starts near the bar top, both channels remain open (continuous lines). The larger the width ratio, the more water flows through the side channel. These results suggest that enlarging the width ratio increases the stability of the bifurcation.

In general, the evolution with constant discharge is relatively fast. When it does not reach a dynamic balance, it reaches the dominant configuration in which one of the parallel channels silts up within the first 14 years.

4.3. Effects of variable discharge

A set of runs was carried out to study the effects of variable discharge on bifurcation stability, considering that flow variations can influence the bar location and geometry as well as the sediment distribution between the two channels. As in the previous set of runs, three different width ratios were considered: $B_1/B_2 = 1:5$ (base-case scenario), $B_1/B_2 = 1:2$, and $B_1/B_2 = 1:1$. The following three starting locations were analysed: 4 (upstream of bar top), 10 (bar top), and 17 (downstream of bar top), see Fig. 7.

The reference case with variable flow started with a flat bed. The bars that formed after 100 years can be recognized from Fig. 13, showing their evolution during the tenth year due to discharge variations. Bars tend to disappear at peak discharge ($Q = 590 \text{ m}^3/\text{s}$), when the width-to-depth ratio is the minimum ($B/h = 15$). At peak discharge low-amplitude migrating bars are observable in the straight reach with the exception of a forced bar near the transverse wall and a strongly damped hybrid bar further downstream at the opposite side. Bars start to reform after the peak discharge since small-amplitude bars are already visible at the end of the flood wave, at a discharge of $Q = 267 \text{ m}^3/\text{s}$, when the width-to-depth ratio has increased to $B/h = 25$. It can be observed that the small migrating bars are gradually suppressed by a series of longer hybrid bars forming downstream of the

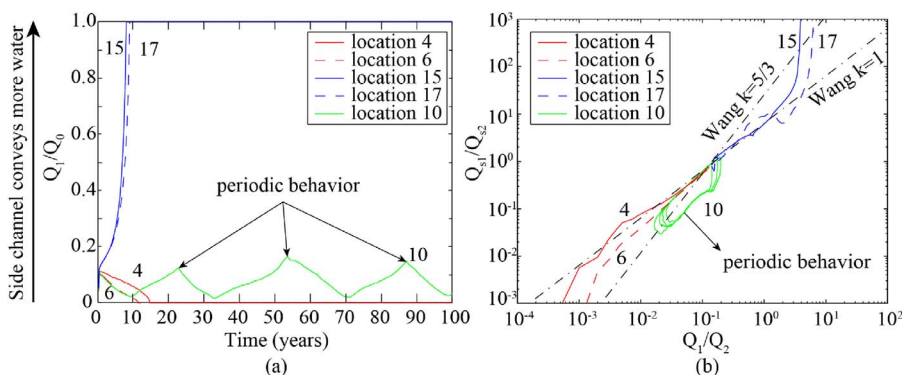


Fig. 10. Temporal variations of discharge and sediment redistribution at the bifurcation. (a) Temporal variation of the ratio between the discharge entering the side channel and the total discharge Q_1/Q_0 . (b) Sediment distribution Q_{s1}/Q_{s2} versus discharge distribution Q_1/Q_2 between side and main channel. Locations 4 and 6 lead to side channel silt up (in red); Locations 15 and 17 lead to side channel erosion (in blue); location 10 leads to a dynamic balance showing a periodic behavior (in green). (For interpretation of the references to color in this figure legend, the reader is referred to the web version of this article.)

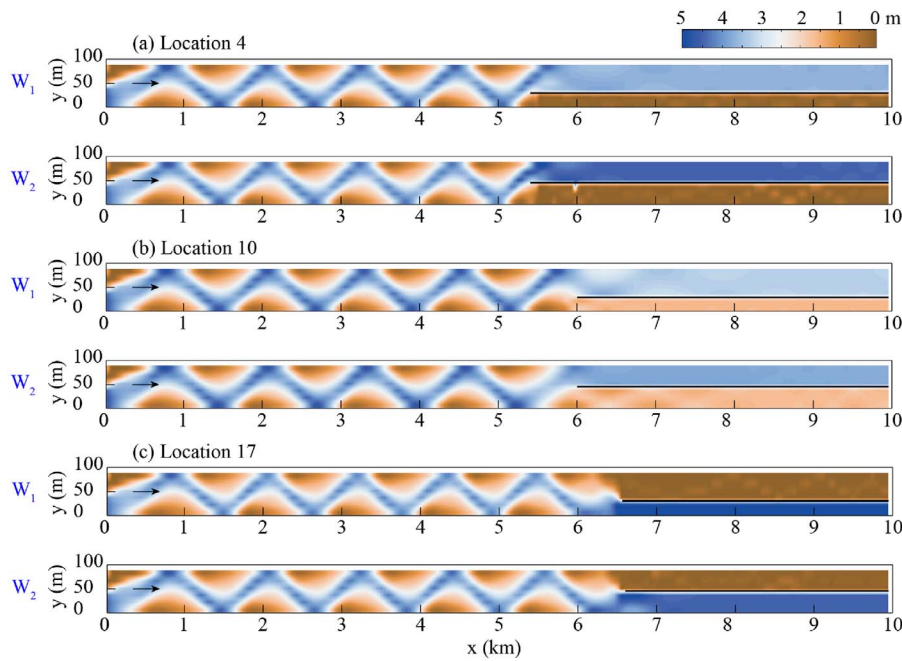


Fig. 11. Results of different width ratios: water depth at the constant discharge of $200 \text{ m}^3/\text{s}$ after 100 years (first 10 km after the transverse dam). (a) Training wall starting at Location 4. (b) Training wall starting at Location 10. (c) Training wall starting at Location 17.

transverse wall. After the period characterized by the average discharge ($Q = 200 \text{ m}^3/\text{s}$), the small migrating bars are still present and with larger amplitude. They are further suppressed in the low-discharge period ($Q = 151 \text{ m}^3/\text{s}$). The results show that the bar wave length increases whereas the bar amplitude decreases with the discharge. This is valid for both hybrid and free migrating bars. Table 4 presents bar development under variable discharge.

The analysis of bar evolution shows that, influenced by the forcing offered by the transverse wall, the first bar on the right side is the most stable one and the second bar on the right side has some variations in shape due to variable discharge. In order to observe clear effects of the variable discharge, the starting locations of the training wall refer to the second bar on the right side. Starting the longitudinal wall near one of the most downstream and variable bars could lead to different conclusions.

The results of the simulations with the longitudinal wall starting from the bed topography at the end of the tenth year of the reference case show bed evolution trends that are similar to the cases with constant discharge (Fig. 14): if the training wall starts in the upstream part of a steady bar the side channel silts up (Fig. 14.a), whereas if the training wall starts in the downstream part of the same bar the side channel deepens (Fig. 14.c). However, if the training wall starts near the bar top, the evolution is similar to the case in which the wall starts

in the upstream part of the bar.

Fig. 14 shows the water depth at the end of the 100th year at low flow for different width ratios. It might give the impression that one of the parallel channels always silts up completely but that is not true, since the plots refer to the final bed configuration at low flow condition. Fig. 15 shows the temporal evolution of the ratio of side-channel discharge to total discharge (Q_1/Q_0). During the first 30 years, both channels remain open. From the 31st year on, both channels remain open during high flow, whereas one of the channels closes during low flow. The parallel-channel system does not find a dynamic equilibrium as occurs with a constant discharge if the training wall starts at Location 10 which is located at 2.2 km from the transverse wall (Fig. 13, dash line). The conveyance of the silting channel slowly diminishes with time to reach a constant value after 70 years. This could be explained by the longitudinal variation of the reference bar shape due to variable discharge (Fig. 13): the location of the initial bar-top is situated in the upstream part of a bar during average to moderate discharge and in a pool at the highest discharge, but for a relatively short duration.

4.4. Sensitivity analysis on the effects of transverse bed slope

A sensitivity analysis was carried out to assess the dependence of bifurcation stability on transverse bed slope, by increasing and

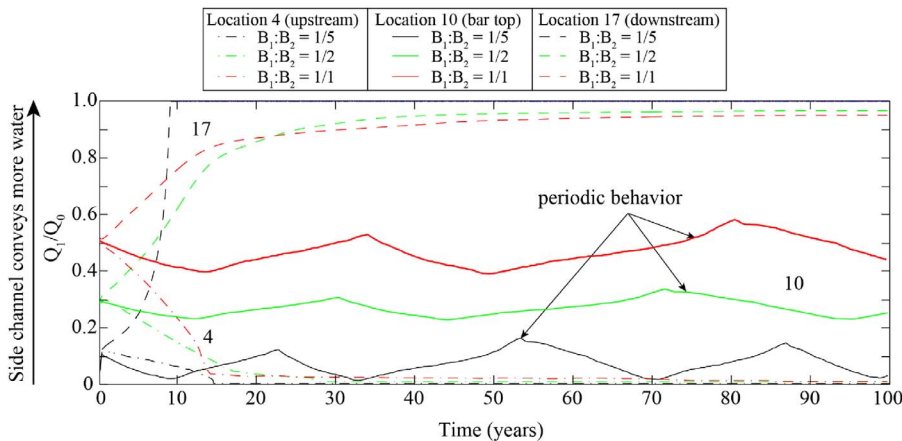


Fig. 12. Temporal evolution of the ratio between the discharge entering the side channel and the total discharge Q_1/Q_0 for different width ratios. The dash-dot lines correspond to the cases in which the training wall starts at the upstream location, the continuous lines to the bar top location, and the dash lines to the downstream location. (For interpretation of the references to color in the text, the reader is referred to the web version of this article.)

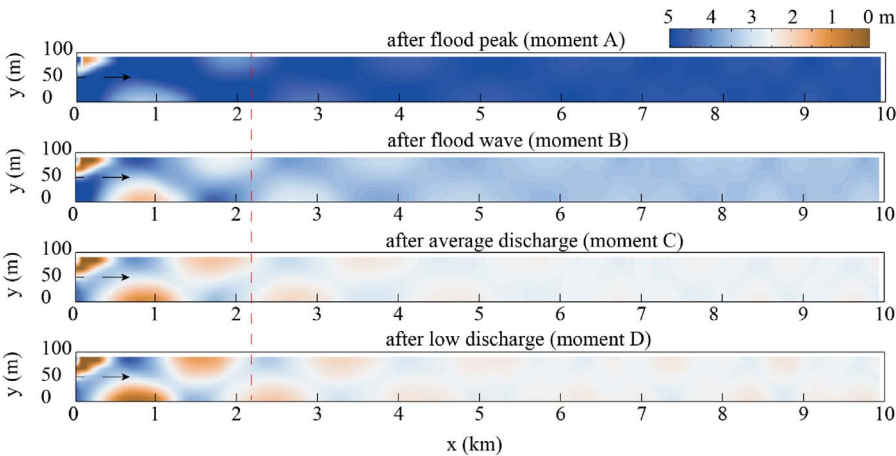


Fig. 13. Reference case without longitudinal wall: evolution of water depth with variable discharge during the 100th year. The yearly hydrograph is shown in Fig. 6. The figure shows the first 10 km after the transverse dam. The dash line identifies the initial location of the second bar top.

Table 4
Bar development under variable discharge.

Q (m ³ /s)	Period	B/h	Hybrid bars		Free migrating bars	
			Amplitude (m)	Wavelength (m)	Amplitude (m)	Wavelength (m)
590	Peak discharge	15	0.5	2200	0.3–1.5	1000–2000
267	End of flood wave	25	0.6–0.8	2000–2100	0.3–2.0	800–1400
200	Average discharge	30	0.9–1.2	1800–1900	0.5–2.5	600–1200
151	Low discharge	36	1.4–1.8	1600–1700	0.8–2.5	600–1400

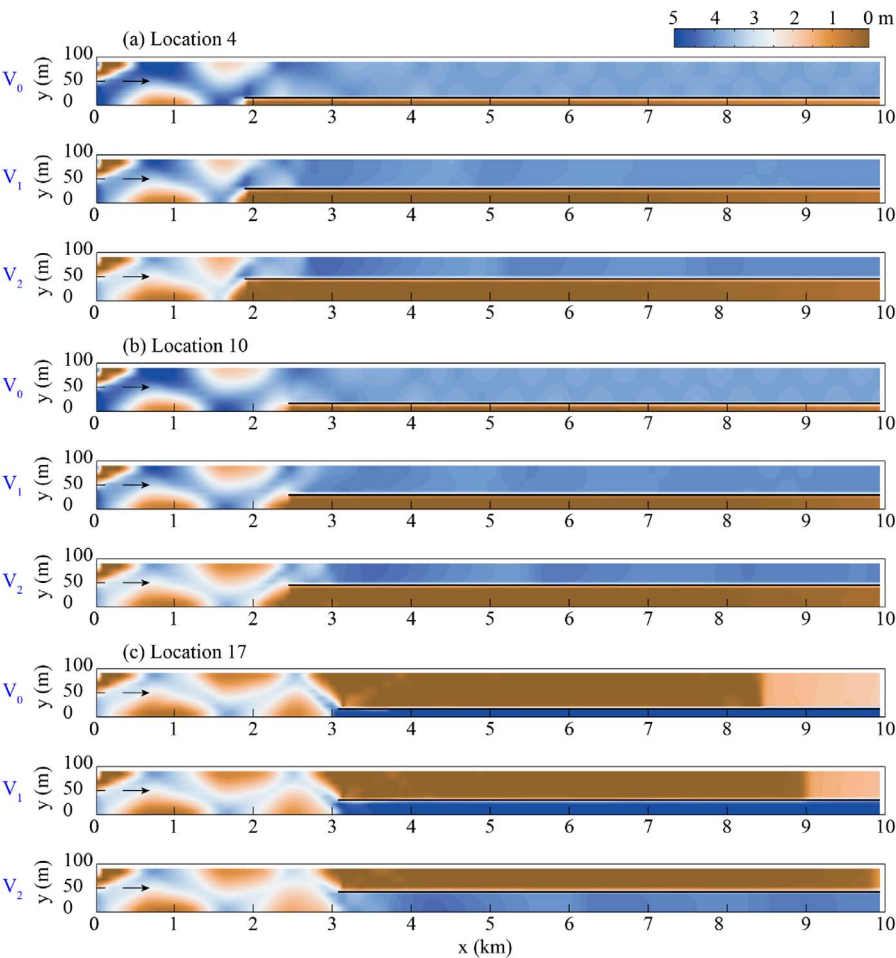
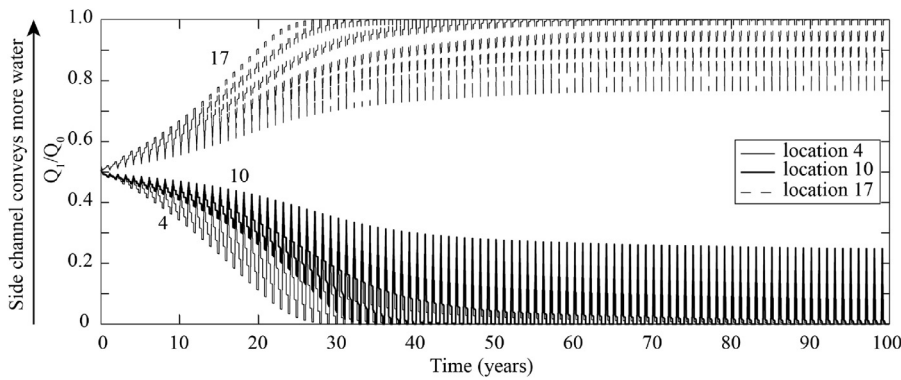


Fig. 14. Results of variable discharge runs for different width ratios: water depth under variable discharge after 100 years. (a) Training wall starting at Location 4 (upstream of bar top). (b) Training wall starting at Location 10 (bar top). (c) Training wall starting at Location 17 (downstream of bar top). The figure shows the first 10 km after the transverse dam.

Fig. 15. Evolution of discharge ratio for $B_1:B_2 = 1:1$.

decreasing its effects on sediment transport direction. This was obtained in the model by applying Koch and Flokstra's (1981) formulation, extended for the effect of bedforms, according to which the function $f(\theta)$ is calculated as:

$$f(\theta) = A_{sh} \theta^{B_{sh}} \left(\frac{D}{h} \right)^{C_{sh}} \quad (3)$$

where A_{sh} , B_{sh} and C_{sh} are calibration coefficients, θ represents the Shields parameter, D is sediment size and h is the normal depth. Among the three parameters, A_{sh} is the most sensitive one. Increasing the value of A_{sh} decreases the effects of transverse slope on sediment transport direction (Schuurman et al., 2013). The value of A_{sh} normally falls in the range 0.5–1.5 and this is the range of values used for the sensitivity analysis, whereas the values of the other calibration coefficients are kept constant: $B_{sh} = 0.5$ and $C_{sh} = 0.3$ (Talmon et al., 1995).

The numerical simulations show that, starting from a flat bed, different values of A_{sh} resulted in different bar characteristics. Analysing the values in Table 5, we can observe that the bar wavelength increases if the bed slope effects increase (decreasing A_{sh}), whereas the opposite trend can be observed for the bar amplitude (stronger bed slope effects result in smaller amplitudes). Based on the equilibrium state, two locations for the starting point of the longitudinal training wall were selected: Location 4 in the upstream part of a bar and Location 17 in the downstream part. The results show that varying the effect of bed slope did not change the final configuration of the bifurcating channels. A training wall starting at Location 4 always resulted in side channel silt-up whereas a training wall starting at Location 17 always resulted in side channel erosion. However, stronger bed slope effects resulted in slower morphological evolution (Table 5), which is probably due to the

smaller bar amplitude resulting in more equal sediment distribution between the channels.

4.5. Sinuous planform

In this section, the numerical simulations represent a sinuous channel with constant discharge of $200 \text{ m}^3/\text{s}$. In the reference case without longitudinal wall, point bars naturally formed near the inner bank of bends (Fig. 16.a). The longitudinal training wall was set only after the point bars were fully-formed. Three locations for its starting point were selected: Location 4, in the upstream part of a point bar, Location 10 near the bar top and Location 17, in its downstream part. The obtained final configurations are shown in Fig. 16. The results are similar to the ones obtained with a straight channel (Fig. 8), indicating that the curvature of the channel and the presence of a relatively strong spiral flow (Ottevanger, 2013) do not change the unstable character of the bifurcation created by a longitudinal training wall. The results indicate that the effects of the spiral flow are less important for the sediment transport direction and the sediment distribution between side and main channel than the main flow deviation and the bed slope caused by the presence of the point bar, at least in the cases examined.

5. Discussion

In the previous sections, attention was paid to rather schematized and idealized examples. For more realistic applications a few aspects should be considered.

Cell drying was obtained numerically in a rather straightforward way, depending on an assigned critical local water depth. We believe

Table 5
Bar development with different magnitude of bed slope effects.

A_{sh}	Bed slope effects	Bar amplitude (m)	Bar wavelength (m)	Duration of morphological evolution (days)	
				Location 4 (Upstream)*	Location 17 (Downstream)**
0.5		0.95	1280	7130	3520
0.6		1.22	1350	6490	3070
0.7		1.82	1290	5760	2910
0.8		1.95	1200	5240	2840
0.9		2.03	1180	4630	2750
1.0		2.08	1175	3860	2630
1.1		2.15	1170	3810	2540
1.2		2.22	1165	3720	2420
1.3		2.25	1160	3660	2370
1.4		2.33	1140	3590	2360
1.5		2.27	1130	3570	2340

* Side channel silt-up

** Side channel erosion

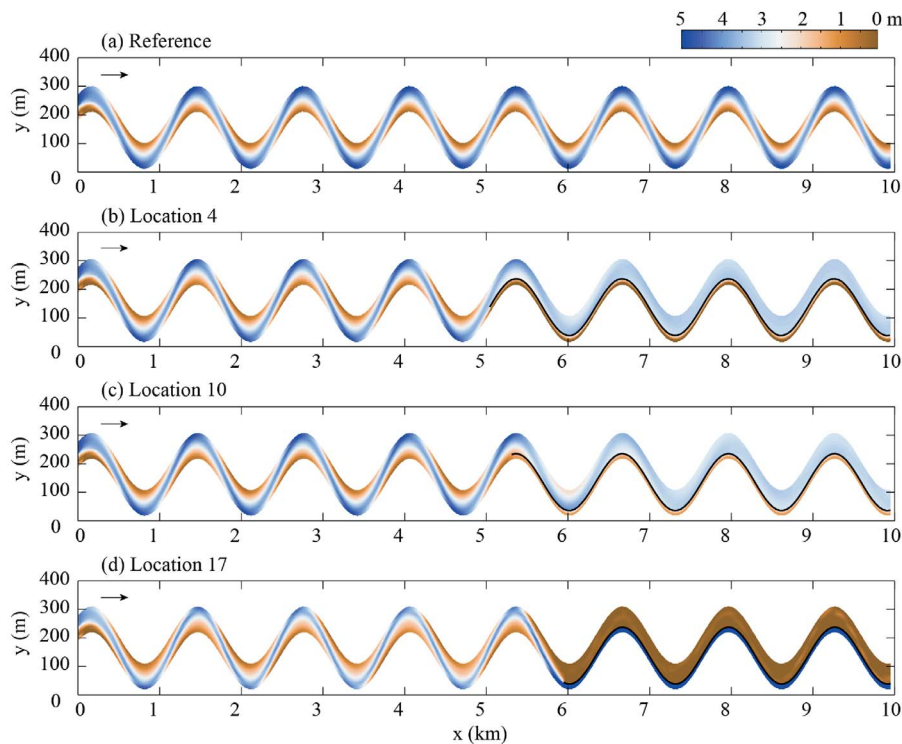


Fig. 16. Sinuous channel simulations: water depth at the constant discharge of $200 \text{ m}^3/\text{s}$ after 100 years. (a) Reference case without longitudinal training wall. (b) Training wall starting at Location 4 (upstream part of a point bar). (c) Training wall starting at Location 10 (bar top). (d) Training wall starting at Location 17 (downstream part of a point bar).

that the areas that become completely dry under constant discharge in the numerical simulations would still convey some water in reality. The experimental study carried out by Le et al. (2018) supports this, because aggrading channels were never found to silt up completely.

All tests were carried out with sediment transported as bed load. The results might be different in presence of substantial amounts of suspended load. This remains open for further research.

Keeping a constant value of the bed roughness, represented in the models by the Chézy coefficient, may have altered the dynamics of the system. The bed roughness should be a function of water depth, becoming gradually higher in the aggrading channel and lower in the deepening one. Similarly the bed roughness should vary with the discharge.

The numerical grid used in the computations contains six cells in the cross-section. Because two-dimensional aspects of water flow and sediment transport are important for bifurcation studies, we also performed other computational tests (not shown here) with 18 cells. The results of the finer grid confirmed the morphological developments obtained with the coarser grid. For this reason, we decided to use the coarser grid, which allowed for the computation of many different scenarios (in total 102 model runs).

An important issue in morphodynamic modelling is the use of a morphological factor (MF) which accelerates the bed development and decreases the computational time. In this study, we applied $\text{MF} = 10$, but only for the cases with constant discharge, after having checked that it does not affect the results in a relevant way. To check this, we performed a computation using $\text{MF} = 1$ (no morphological acceleration) and obtained after 10 years results that did not differ, when plotted, in an observable way from the results of one year using $\text{MF} = 10$. For variable discharge, we represented the yearly hydrograph in a schematic way and performed the computation without any morphological acceleration. In this way we could distinguish the yearly effects of the variable discharge.

In computations with a constant discharge, the time corresponding to the morphological developments is merely theoretical. Using a morphological acceleration factor larger than 1 (after having checked that it does not affect the results) therefore does not affect the

interpretation of the results, since the link with time is not clear anyway. With variable discharge, especially if a yearly hydrograph is used, applying a morphological acceleration factor larger than 1 creates an unclear distortion of time and hampers the interpretations of time developments. For this reason, we discourage the use of morphological acceleration in computations with variable discharge.

Redolfi et al. (2016) investigated the stability of a symmetrical bifurcation under steady flow conditions, disregarding the presence of alternate bars in the main channel. This symmetrical configuration becomes unstable if the original (not yet bifurcated) channel is at super-resonant conditions, because due to morphodynamics influence, a steady alternate bar forms just upstream of the bifurcation point. This bar tends to unbalance the flow and sediment partition between the bifurcating channels.

In the unsteady flow computations performed here, the width-to-depth ratio falls below the critical value for bar formation during peak flows and for this reason bars tend to disappear (Fig. 13). At the end of the flood wave hybrid bars are incipient and short migrating bars are present. Hybrid bars are fully developed after the low-flow period, although some bar irregularities are present due to the interactions with remains of free bars. The conditions at average discharge, occurring after the flood wave, are close to resonance and at the lowest discharge the systems is super-resonant. According to Zolezzi and Seminara (2001), upstream morphodynamic influence may occur only at the lowest flow rates. However, we do not observe any steady bar interfering with hybrid bars near the bifurcation at the end of the low-flow period. This is a sign of possible hybrid-bar dominance. As a consequence, we can conclude that upstream morphodynamic influence does not affect bifurcation stability at the conditions considered in this study.

Hypothetically, if super-resonant conditions were present for a longer period, i.e. also at higher discharges, a steady bar might develop near the bifurcation. In this case, the stability of the channel system would be determined by the competition between the steady bar at the node and the hybrid bars in the channel. Further investigations are needed to show at which conditions one of the two would prevail.

- 3.15.34158 28, May 2014, https://oss.deltares.nl/documents/183920/185723/Delft3D-FLOW_User_Manual.pdf.
- Duró, G., Crosato, A., Tassi, P., 2015. Numerical study on river bar response to spatial variations of channel width. *Adv. Water Resour.* 93, 21–38. <http://dx.doi.org/10.1016/j.advwatres.2015.10.003>.
- Engelund, F., 1970. Instability of erodible beds. *J. Fluid Mech.* 42 (3), 225–244.
- Engelund, F., Hansen, E., 1967. A Monograph on Sediment Transport in Alluvial Streams. Da. Tech. Press, Copenhagen, Denmark.
- Engelund, F., Skovgaard, O., 1973. On the origin of meandering and braiding in alluvial streams. *J. Fluid Mech.* 57 (2), 289–302.
- Flokstra, C., 1985. De invloed van knooppuntsrelaties op de bodemligging bij splitsingspunten. Waterloopkundig Laboratorium (WL | Delft Hydraulics), Delft, the Netherlands Report R2166 (in Dutch).
- Fredsoe, J., 1978. Meandering and braiding of rivers. *J. Fluid Mech.* 84 (4), 609–624.
- Hansen, E., 1967. On the formation of meanders as a stability problem. Coastal Engineering, Laboratory, Technical University Denmark, Lyngby, Denmark, pp. 9 Progress Report. 13.
- Hirose, K., Hasegawa, K., Meguro, H., 2003. Experiments and analysis on mainstream alternation in a bifurcated channel in mountain rivers. In: Proceedings of Third International Conference on River, Coastal and Estuarine Morphodynamics, Barcelona, Spain, 1–5 September 2003, pp. 571–583.
- Kleinhans, M.G., Jagers, H.R.A., Mosselman, E., Sloff, C.J., 2008. Bifurcation dynamics and avulsion duration in meandering rivers by one-dimensional and three-dimensional models. *Water Resour. Res.* 44 (W08454). <http://dx.doi.org/10.1029/2007WR005912>.
- Koch, F.G., Flokstra, C., 1981. Bed level computations for curved alluvial channels. In: Proceeding of 19th Congress IAHR, New Delhi, India, February 1981, Also Delft Hydraulics Publication No. 240, November 1980.
- Lanzoni, S., 2000. Experiments on bar formation in a straight flume: 1. uniform sediment. *Water Resour. Res.* 36, 3337–3349.
- Le, T.B., Crosato, A., Uijttewaal, W.S.J., 2018. Long-term morphological developments of river channels separated by a longitudinal training wall. *Adv. Water Resour.* <http://dx.doi.org/10.1016/j.advwatres.2018.01.007>.
- Mosselman, E., Tubino, M., Zolezzi, G., 2006. The overdeepening theory in river morphodynamics: two decades of shifting interpretations. In: Ferreira, R.M.L., Alves, E.C.T.L., Leal, J.G.A.B., Cardoso, A.H. (Eds.), *River Flow 2006*, Lisbon, 6–8 Sept. 2006. Taylor & Francis, London, pp. 1175–1181 ISBN 978-0-415-40815-8.
- Mosselman, E., Le, T.B., 2016. Five common mistakes in fluvial morphodynamic modeling. *Adv. Water Resour.* 93, 15–20. <http://dx.doi.org/10.1016/j.advwatres.2015.07.025>.
- Ottevanger, W., 2013. Modelling and parameterizing the hydro- and morphodynamics of curved open channels. PhD thesis, Faculty of Civil Engineering and Geosciences. Department of Hydraulic Engineering. Delft University of Technology. ISBN:9789461919250..
- Parker, G., 1976. On the cause and characteristic scales of meandering and braiding in rivers. *J. Fluid Mech.* 76 (3), 457–479.
- Redolfi, M., Zolezzi, G., Tubino, M., 2016. Free instability of channel bifurcations and morphodynamic influence. *J. Fluid Mech.* 799, 476–504. <http://dx.doi.org/10.1017/jfm.2016.389>.
- Schuurman, F., Marra, W.A., Kleinhans, M.G., 2013. Physics-based modeling of large braided sand-bed rivers: bar pattern formation, dynamics and sensitivity. *J. Geophys. Res. Earth Surf.* 118, 2509–2527. <http://dx.doi.org/10.1002/2013JF00>.
- Singh, U., Crosato, A., Giri, S., Hicks, M., 2017. Sediment heterogeneity and mobility in the morphodynamic modelling of gravel-bed braided rivers. *Adv. Water Resour.* Elsevier 104, 127–144. <http://dx.doi.org/10.1016/j.advwatres.2017.02.005>. 2017.
- Struiksma, N., Olesen, K., Flokstra, C., Vriend, H.D., 1985. Bed deformation in curved alluvial channels. *J. Hydr. Res.* 23 (1), 57–79.
- Struiksma, N., Crosato, A., 1989. Analysis of a 2 D bed topography model for rivers. In: Ikeda, S., Parker, G. (Eds.), *River Meandering* 12. AGU, Washington, DC, pp. 153–180.
- Talmon, A.M., Struiksma, N., van Mierlo, M.C.L.M., 1995. Laboratory measurements of the direction of sediment transport on transverse alluvial-bed slopes. *J. Hydr. Res.* 33 (4), 495–517.
- Van der Mark, C.F., Mosselman, E., 2013. Effects of helical flow in one-dimensional modelling of sediment distribution at river bifurcations. *Earth Surf. Process. Landf.* 38, 502–511. <http://dx.doi.org/10.1002/esp.3335>.
- Wang, Z.B., Fokkink, R.J., de Vries, M., Langerak, A., 1995. Stability of river bifurcations in 1D morphodynamic models. *J. Hydr. Res.* 33 (6), 739–750.
- Zolezzi, G., Seminara, G., 2001. Downstream and upstream influence in river meandering. part one: general theory and application of overdeepening. *J. Fluid Mech.* 438, 183–211.
- Zolezzi, G., Guala, M., Termini, D., Seminara, G., 2005. Experimental observations of upstream overdeepening. *J. Fluid Mech.* 531, 191–219. <http://dx.doi.org/10.1017/S0022112005003927>.